Core-level photoelectron spectroscopy study of the Au/Si(111) 5×2, α-$\sqrt{3}\times\sqrt{3}$, β-$\sqrt{3}\times\sqrt{3}$, and 6×6 surfaces

H. M. Zhang,[1] T. Balasubramanian,[2] and R. I. G. Uhrberg[1]
[1]*Department of Physics and Measurement Technology, Linköping University, S-581 83 Linköping, Sweden*
[2]*MAX-lab, Lund University, Box 118, S-221 00 Lund, Sweden*
(Received 30 May 2001; published 21 December 2001)

Submonolayer coverages of Au on Si(111), known as the 5×2, α-$\sqrt{3}\times\sqrt{3}$, β-$\sqrt{3}\times\sqrt{3}$, $2\sqrt{21}\times2\sqrt{21}$, and 6×6 surfaces, have been investigated by low-energy electron diffraction and photoelectron spectroscopy. Three Si $2p$ surface components on the 5×2 surface, and four surface components on the α-$\sqrt{3}\times\sqrt{3}$, quenched β-$\sqrt{3}\times\sqrt{3}$, and 6×6 surfaces have been identified by surface sensitive high resolution core-level spectroscopy. The photoemission data of the α-$\sqrt{3}\times\sqrt{3}$, the 6×6 and the quenched β-$\sqrt{3}\times\sqrt{3}$ phases are discussed in terms of extra Au adatoms on the $\sqrt{3}\times\sqrt{3}$ surface described by the ideal 1 ML conjugate honeycomb chained trimer model. The similarity between the 6×6 and the quenched β-$\sqrt{3}\times\sqrt{3}$ surface is obvious from the decomposition of the Si $2p$ spectra, suggesting an order-disorder relation.

DOI: 10.1103/PhysRevB.65.035314 PACS number(s): 68.35.−p, 73.20.−r, 79.60.−i

I. INTRODUCTION

By depositing Au on a Si(111) surface, several reconstructions can be formed for coverages up to about 1 monolayer (ML), i.e., 5×2, α-$\sqrt{3}\times\sqrt{3}$, β-$\sqrt{3}\times\sqrt{3}$, $2\sqrt{21}\times2\sqrt{21}$, and 6×6. In contrast to many other metal-induced superstructures on Si(111), the Au/Si(111) surfaces contain a certain amount of structural disorder, which results in streaky $2\times$ diffraction in the 5×2 low energy electron diffraction (LEED) patterns, diffuse $\sqrt{3}\times$ diffraction spots for α-$\sqrt{3}\times\sqrt{3}$, and ringlike diffraction in the case of β-$\sqrt{3}\times\sqrt{3}$. The $2\sqrt{21}\times2\sqrt{21}$ and 6×6 reconstructions, on the other hand, exhibit only sharp diffraction spots and seem to be quite well ordered.

Extensive research has been carried out on the Au/Si(111) surfaces (such as 5×2 and $\sqrt{3}\times\sqrt{3}$) throughout the years. Despite this effort, no consensus has been obtained regarding structure models or Au coverage. In recent years, two new atomic models of the 5×2 phase have been proposed by Marks and Plass[1,2] and Hasegawa *et al.*[3,4] Both models[2,3] contain two Au rows in a 5×2 periodicity, and additional Au atoms corresponding to the bright protrusions observed in the STM images.[5] The two models differ in the number and the arrangement of the Au and Si atoms in the reconstructed layers. The Au coverage of the two 5×2 models are about 0.43 ML.

In a previous study of the $\sqrt{3}\times\sqrt{3}$ surface, Ding *et al.*[6] proposed the conjugate honeycomb chained trimer (CHCT-1) model with a nominal coverage of 1 ML for the Au/Si(111) $\sqrt{3}\times\sqrt{3}$ surface. This model is related to the HCT-1 model of the Ag/Si(111) $\sqrt{3}\times\sqrt{3}$ surface. Later, based on transmission electron microscopy (TEM), Plass and Marks[1,2,7,8] supported the missing top layer twisted trimer (MTLTT) model proposed by Chester and Gustafsson.[9] Either a ''vacancy'' type of domain wall (formed by a Si double layer without gold adatoms) or a ''neutral'' type were suggested (formed by a missing top layer with single or multiple gold adatoms). The α-$\sqrt{3}\times\sqrt{3}$, β-$\sqrt{3}\times\sqrt{3}$, and 6×6 phases have also been studied in detail with scanning tunneling microscopy (STM).[10–13] It has been confirmed that the domain wall density of the $\sqrt{3}\times\sqrt{3}$ surface becomes higher as the Au coverage increases, and that crystallization of the domain wall structure results in the 6×6 phase at a Au coverage near 1 ML.[12,13] Obviously, several questions arise about the domain wall structure in connection to 1 ML $\sqrt{3}\times\sqrt{3}$ models. For instance, how can the MTLTT or the CHCT-1 model explain the widely observed low coverage ($\sim$0.8 ML) $\sqrt{3}\times\sqrt{3}$ phase if the domain walls contain more Au atoms than the well-ordered $\sqrt{3}\times\sqrt{3}$ parts? For the 6×6 phase, an interesting pseudopentagonal glass model was proposed by Marks *et al.*,[14,15] based on surface x-ray diffraction data. In this model, a network of incomplete pentagons and trimers forms from the connection of every Au trimer to additional Au atoms. In earlier photoemission studies, Okuda and co-workers[16,17] have systematically studied the 5×2, α-$\sqrt{3}\times\sqrt{3}$, β-$\sqrt{3}\times\sqrt{3}$, and 6×6 Au/Si(111) surfaces. Their spectra showed rather broad Si $2p$ core-level line shapes, which inevitably led to an uncertainty in the decomposition of the spectra.

In this study, we report results from LEED and high resolution Si $2p$ core-level photoelectron spectroscopy. More surface components are found on the different Au/Si(111) surfaces by high resolution Si $2p$ core-level spectroscopy compared to the previous work.[16,17] The LEED images clearly show the 5×2, α-$\sqrt{3}\times\sqrt{3}$, β-$\sqrt{3}\times\sqrt{3}$, $2\sqrt{21}\times2\sqrt{21}$, 6×6, and the quenched β-$\sqrt{3}\times\sqrt{3}$ surface reconstructions. The β-$\sqrt{3}\times\sqrt{3}$ and the quenched β-$\sqrt{3}\times\sqrt{3}$ surfaces are almost identical, as evidenced by their LEED patterns and photoemission spectra. Core-level photoelectron spectroscopy shows a clear similarity between the 6×6 and the quenched β-$\sqrt{3}\times\sqrt{3}$ phases. This result indicates an order to disorder transition going from the 6×6 to the quenched β-$\sqrt{3}\times\sqrt{3}$ phase.

II. EXPERIMENTAL DETAILS

The photoemission study was performed at beam line 33 at the Max-I synchrotron radiation facility in Lund, Sweden. The Si $2p$ core-level spectra were obtained at an energy resolution of $\approx$90 meV with an angular resolution of $\pm2°$.

LEED images were taken with a CCD camera setup. The pressure of the UHV system was around 4×10^{-10} Torr during evaporation and 1×10^{-10} Torr during data collection. The Si(111) samples cut from a single crystal wafer (Sb doped, 3 Ω cm) were preoxidized by an etching method and cleaned *in-situ* by stepwise direct current heating up to 930 °C. This procedure resulted in a clean and well-ordered surface, as evidenced by the strong surface state emission and a sharp 7×7 LEED pattern. Au was evaporated onto the Si(111) surface from a tungsten filament source calibrated by a quartz crystal monitor. Here, it is appropriate to consider the uncertainty in the Au coverage. An error on the order of 5–10% is probably a realistic estimate. Evaporation of ~0.5 ML of Au followed by annealing at ≈580 °C for 5 min. resulted in a sharp 5×1 LEED pattern with streaklike $2\times$ diffraction [Fig. 1(a)]. Evaporation of ~0.9 ML of Au followed by the same annealing procedure gave sharp $\sqrt{3}\times$ LEED spots surrounded by cloudlike diffraction [Fig. 1(b), α-$\sqrt{3}\times\sqrt{3}$]. The same annealing procedure of ~1.0 ML of Au resulted in sharp $\sqrt{3}\times$ LEED spots surrounded by ringlike diffraction [Fig. 1(c), β-$\sqrt{3}\times\sqrt{3}$]. However, the same annealing temperature and time, but ended by slow cooling to room temperature (RT), gave a new $2\sqrt{21}\times2\sqrt{21}$ LEED pattern [Fig. 1(d)]. Finally, ~1.1 ML of Au followed by annealing at ≈700 °C for 1 minute, and slow cooling to RT, led to the formation of a well-defined 6×6 LEED pattern [Fig. 1(e)]. Interestingly, the same annealing but ended by rapid cooling resulted in a quenched β-$\sqrt{3}\times\sqrt{3}$ LEED pattern [Fig. 1(f)].

III. RESULTS AND DISCUSSION

The LEED images in Fig. 1 clearly distinguish the surface reconstructions of the 5×2, α-$\sqrt{3}\times\sqrt{3}$, β-$\sqrt{3}\times\sqrt{3}$, $2\sqrt{21}\times2\sqrt{21}$, 6×6, and the quenched β-$\sqrt{3}\times\sqrt{3}$ Au/Si(111) surfaces. The weak $2\times$ streaks in Fig. 1(a) suggest a certain disorder in the 5×2 unit cell or mismatch along the $2\times$ direction. In the case of α-$\sqrt{3}\times\sqrt{3}$, Fig. 1(b) shows diffuse or cloudlike diffraction around $\sqrt{3}\times$ spots, which actually has a hexagonal shape and consists of six small diffraction spots. In comparison with the 6×6 LEED pattern, the distances between these six spots are much smaller, indicating an ordering in real space with a long repeating distance. Here, it is interesting to compare our LEED images with the previous STM studies.[10–13] It was suggested that the size of the $\sqrt{3}\times$ LEED spots reflects the domain size of the $\sqrt{3}\times\sqrt{3}$ areas. A possible situation could be that the α-$\sqrt{3}\times\sqrt{3}$ surface, which has a low density of domain walls, already has some long range ordering of these domain walls. One can notice that there is also streaky diffraction along the $\sqrt{3}\times$ directions, suggesting some mismatch between the surface unit cells. In Fig. 1(c), the β-$\sqrt{3}\times\sqrt{3}$ phase shows a hexagonal, ringlike diffraction with a distance close to the $6\times$ distance, and the $\sqrt{3}\times$ streaky diffraction has disappeared. The $\sqrt{3}\times$ spots have become quite sharp compared to the α-$\sqrt{3}\times\sqrt{3}$ LEED pattern. The hexagonal ringlike structure could come from an ordering of the domain walls, which is consistent with STM observations.[10–13] Furthermore, a detailed inspection of the LEED images shows that the ringlike diffraction of the β-$\sqrt{3}\times\sqrt{3}$ phase resembles that of a $\sqrt{39}\times\sqrt{39}$ reconstruction [Fig. 1(g)], which has been observed for the Ag/Ge(111) system.[18,19] In other words, the β-$\sqrt{3}\times\sqrt{3}$ phase may be called a pseudo-$\sqrt{39}\times\sqrt{39}$ phase. The $2\sqrt{21}\times2\sqrt{21}$ phase [Figs. 1(d), 1(h)], which was first reported in Ref. 13, seems to be a well-defined surface. By applying fast or slow cooling procedures, we find that the $2\sqrt{21}\times2\sqrt{21}$ phase can be reversibly transformed into the β-$\sqrt{3}\times\sqrt{3}$ phase, which is in contrast to the observation in Ref. 13.

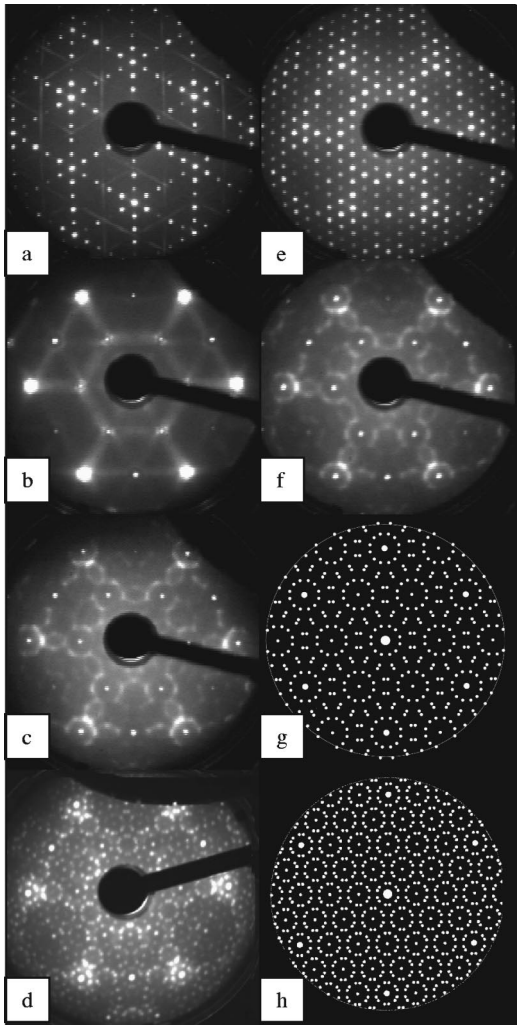

FIG. 1. LEED patterns of the Au/Si(111) surfaces as a function of Au coverage θ (100 K). (a) $\theta\approx0.5$ ML, 5×2 phase, 98 eV; (b) $\theta\approx0.9$ ML, α-$\sqrt{3}\times\sqrt{3}$ phase, 74 eV; (c) $\theta\approx1.0$ ML, β-$\sqrt{3}\times\sqrt{3}$ phase, 74 eV; (d) $\theta\approx1.0$ ML, $2\sqrt{21}\times2\sqrt{21}$ phase, 74 eV; (e) $\theta\approx1.1$ ML, 6×6 phase, 74 eV; (f) $\theta\approx1.1$ ML, quenched β-$\sqrt{3}\times\sqrt{3}$ phase, 74 eV. (g) Schematic LEED pattern of the $\sqrt{39}\times\sqrt{39}$ phase; (h) schematic LEED pattern of the $2\sqrt{21}\times2\sqrt{21}$ phase.

Here, it is interesting to compare the different Au/Si(111) surfaces to the closely related Ag/Si(111) and Ag/Ge(111) surfaces. The Ag/Si(111) and Ag/Ge(111) surfaces show almost the same surface reconstructions at coverages above 1 ML. The reconstructions change from $\sqrt{3}\times\sqrt{3}$ via $\sqrt{21}$

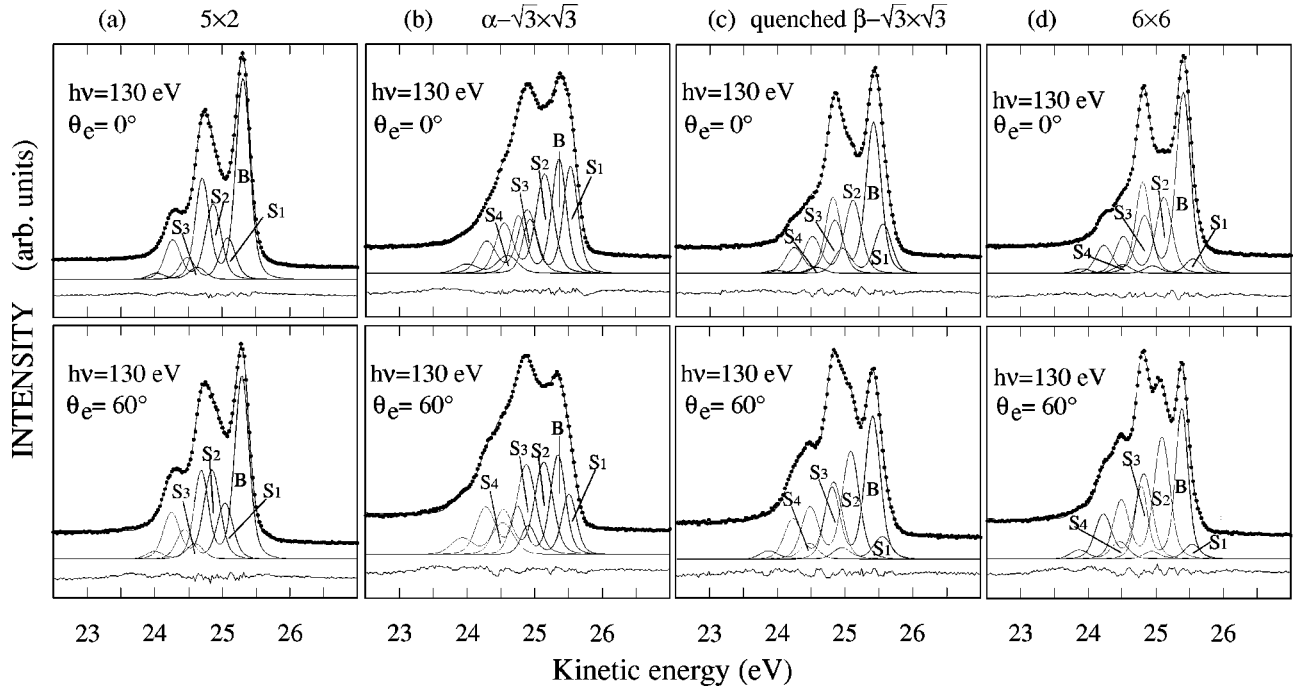

FIG. 2. Si $2p$ core-level spectra recorded from the Au/Si(111) surfaces at normal emission and a surface sensitive angle of 60° (100 K). All spectra were obtained with a photon energy of 130 eV at an incident angle of 45°. The solid curves show the components that were used to fit the experimental data (solid circles). (a) 5×2 phase; (b) α-$\sqrt{3}\times\sqrt{3}$ phase; (c) quenched β-$\sqrt{3}\times\sqrt{3}$ phase; (d) 6×6 phase.

$\times\sqrt{21}$ to 6×6 for Ag/Si(111) and from $\sqrt{3}\times\sqrt{3}$ via $\sqrt{39}\times\sqrt{39}$ to 6×6 for Ag/Ge(111) with increasing Ag coverage. Thus, it may not be too surprising that Au/Si(111) exhibits $2\sqrt{21}\times2\sqrt{21}$ and 6×6 reconstructions and a $\sqrt{39}\times\sqrt{39}$-like periodicity at coverages around 1 ML. The 6×6 phase in Fig. 1(e) shows a well-defined reconstruction except for relatively strong $\sqrt{3}\times$ LEED spots for most energies [except for 74 eV in Fig. 1(e)]. Just by applying a different annealing process, the quenched β-$\sqrt{3}\times\sqrt{3}$ phase [Fig. 1(f)] was obtained from the 6×6 surface. One interesting observation is that the LEED pattern of the β-$\sqrt{3}\times\sqrt{3}$ phase (1.0 ML) is almost identical to the quenched β-$\sqrt{3}\times\sqrt{3}$ phase (1.1 ML), although their corresponding well-ordered surfaces are the $2\sqrt{21}\times2\sqrt{21}$ and 6×6 phases, respectively. This is consistent with STM observations that the β-$\sqrt{3}\times\sqrt{3}$ structure is actually quite similar to the $2\sqrt{21}\times2\sqrt{21}$ and the 6×6 phases regarding the local atomic arrangement.[13] However, the most interesting phenomena are the transition between 6×6 and its quenched β-$\sqrt{3}\times\sqrt{3}$ phase and the transition between the β-$\sqrt{3}\times\sqrt{3}$ and the $2\sqrt{21}\times2\sqrt{21}$ phases. Below, we limit our discussion to the former case.

By measuring the total width of the valence band spectra ($h\nu=21.2$ eV, -10 V sample bias), from the low energy cutoff to the Fermi level (E_F), we have determined the work function for the different surfaces. The values obtained for the 7×7, 5×2, α-$\sqrt{3}\times\sqrt{3}$, β-$\sqrt{3}\times\sqrt{3}$, and 6×6 phases are 4.64, 4.98, 5.19, 4.91, and 4.86 eV, respectively. The pinning position of the Fermi level with respect to the valence band maximum E_F-E_V was estimated by comparing bulk sensitive Si $2p$ core-level spectra obtained at a photon energy of 108 eV. Using a reference value of 0.63 eV for the Si(111)7×7 surface[20] we obtain E_F-E_V values of 0.30, 0.13, 0.30, and 0.34 eV for the 5×2, α-$\sqrt{3}\times\sqrt{3}$, β-$\sqrt{3}\times\sqrt{3}$, and 6×6 phases, respectively. Figure 2 shows high resolution Si $2p$ core-level spectra obtained from the 5×2, α-$\sqrt{3}\times\sqrt{3}$, quenched β-$\sqrt{3}\times\sqrt{3}$ and 6×6 Au/Si(111) surfaces at two emission angles. In the fitting program, we have used a Gaussian width (FWHM) of 0.17–0.22 eV and a Lorentzian width (FWHM) of 0.085 eV for the bulk Si $2p$ component. An integrated background function was also used to obtain generally better fits throughout the whole energy and emission angle ranges. In the spectra of the 5×2 phase in Fig. 2(a), it is necessary to introduce *two* surface components S_1 and S_2 to fit the valley instead of *one* broad component as in Ref. 16. From the asymmetric shapes of the raw spectra at the low kinetic energy side, it is obvious that they must also contain one more component (S_3). The fitting results are presented in Table I. The core-level shifts of S_1, S_2, and S_3 are 0.24, 0.44, and 0.69 eV with respect to the bulk component. A positive shift means a shift to higher binding energy. The intensity percentages indicate the relative amount of different Si sites on the Au/Si(111) surface. The two new structure models of the 5×2 phase proposed by Marks and Plass[1,2] and Hasegawa *et al.*[3,4] both have Au double rows separated by a $5\times$ distance. Each double row consists of two linear chains of Au atoms. If one only considers Si sites, which are significantly different from bulk sites, one finds that both models have two major sites. There is one type of Si site located within a Au double row, which has three dangling bonds. Another Si site, with one dangling bond, is located between the Au double rows. It seems rea-

TABLE I. Parameters for the components used to fit the Si $2p$ core-level spectra of the 5×2, α-$\sqrt{3}\times\sqrt{3}$, quenched β-$\sqrt{3}\times\sqrt{3}$, and 6×6 Au/Si(111) surfaces shown in Fig. 2. All energies are in eV. The branching ratios vary from 0.48 to 0.52 for the different components.

	Au/Si(111) 5×2		Au/Si(111) α-$\sqrt{3}\times\sqrt{3}$		Au/Si(111) β-$\sqrt{3}\times\sqrt{3}$		Au/Si(111) 6×6	
	0°	60°	0°	60°	0°	60°	0°	60°
Spin-orbit split	0.602	0.602	0.602	0.602	0.602	0.602	0.602	0.602
Lorentzian width	0.085	0.085	0.085	0.085	0.085	0.085	0.085	0.085
Bulk component (B)								
Gaussian width	0.198	0.201	0.203	0.216	0.215	0.219	0.198	0.172
Bulk core-level shift	−0.344		−0.498		−0.281		−0.293	
Surface component (S1)								
Core-level shift	0.226	0.250	−0.170	−0.164	−0.141	−0.142	−0.143	−0.155
Gaussian width	0.222	0.230	0.203	0.208	0.243	0.256	0.234	0.232
Intensity (%)	12.1	16.4	24.5	13.6	15.2	6.0	4.0	3.5
Surface component (S2)								
Core-level shift	0.440	0.442	0.212	0.210	0.304	0.326	0.287	0.295
Gaussian width	0.225	0.237	0.256	0.270	0.243	0.250	0.234	0.232
Intensity (%)	24.5	28.3	26.2	25.7	22.4	29.9	22.7	32.7
Surface component (S3)								
Core-level shift	0.679	0.694	0.469	0.470	0.573	0.580	0.574	0.563
Gaussian width	0.235	0.246	0.275	0.280	0.244	0.253	0.250	0.240
Intensity (%)	3.5	4.3	17.9	27.0	16.6	22.3	18.0	24.7
Surface component (S4)								
Core-level shift			0.764	0.819	0.849	0.941	0.900	0.927
Gaussian width			0.310	0.330	0.250	0.260	0.250	0.250
Intensity (%)			5.0	10.1	1.4	4.3	4.0	4.6

sonable to assign S_2 to the Si atoms with three dangling bonds due to the large core-level shift, while S_1 probably corresponds to the Si atoms with one dangling bond which may bond to a Au adatom. The small component S_3 might be related to surface defects. Due to the complexity of the two structure models and the fact that only two major surface shifted components are observed, we do not find it meaningful to pursue any further discussion of the core-level data and the models in this paper.

Figure 2(b) shows the Si $2p$ core-level spectra obtained from the α-$\sqrt{3}\times\sqrt{3}$ phase at two emission angles. The higher surface sensitivity at 60° emission compared to normal emission results in a clear difference in the raw spectra. Compared to the 5×2 surface one has to use one more component (S_1) at the high kinetic energy side to obtain a high quality fit. The surface components S_2 and S_3 have to be introduced in order to fit the valley of the spectra. Judged from the asymmetric shapes of the raw spectra at the lower kinetic energy side, it is obvious that there is one more component (S_4). The fitting results of the α-$\sqrt{3}\times\sqrt{3}$ phase are presented in Table I. There are *four* surface components (S_1, S_2, S_3, and S_4) instead of *two* broad components in the Si $2p$ spectra of the α-$\sqrt{3}\times\sqrt{3}$ surface as suggested in Ref. 16. The core-level shifts of S_1, S_2, S_3, and S_4 are −0.17, 0.21, 0.47, and 0.80 eV with respect to the bulk component. In the ideal 1 ML CHCT-1 model (Fig. 3),[6] which is popular for the α-$\sqrt{3}\times\sqrt{3}$ surface, the central parts are Au and Si trimers. This model is consistent with the observation of a number of different surface components. One component may originate from the Si trimer atoms (A) of the first layer, and a second component can be associated with the second layer Si atoms (B), which bond directly to the upper Si trimer atoms. The third layer Si atoms (C), which are located below the center of a Si trimer, and the third layer Si atoms (D), which are located below the center of a Au trimer may give rise to a third and a fourth component. We tentatively assign the surface components S_3, S_2, and S_1 [Fig. 2(b)] to the A, B, and C Si sites (Fig. 3). The reason why S_3 is assigned to the Si trimer (A) is the strong Au-Si bonds and the fact that Au has a larger electronegativity than Si.[6] Thus the Si trimer might have a positive charge and the corresponding surface component should shift to higher binding energy compared to the bulk component. In similarity, the third layer Si atoms (C), which are below the centers of the Si trimers, could give rise to the low binding energy component (S_1), due to a polarization effect. It is also reasonable that the second layer Si atoms (B), which bond directly to the upper Si trimer atoms, can be associated with S_2 which is shifted slightly toward higher binding energy compared to the bulk component. However, the large shift to high binding energy of S_4 is difficult to explain. It might not be correct to associate the S_4 component with a specific Si site of the model, since it always makes just a small contribution to the Si $2p$ spectra and it cannot be fitted uniquely. S_4 might instead be related to surface defects. An interesting observation is the behavior of the S_1 component, which shows a lower intensity when using a higher emission angle. The intensities of the different Si $2p$ components of the α-$\sqrt{3}\times\sqrt{3}$ phase show strong diffraction effects. Figure 4 shows a set of Si $2p$ spectra for various emission angles in the range 0° to 60°. The diffraction effect

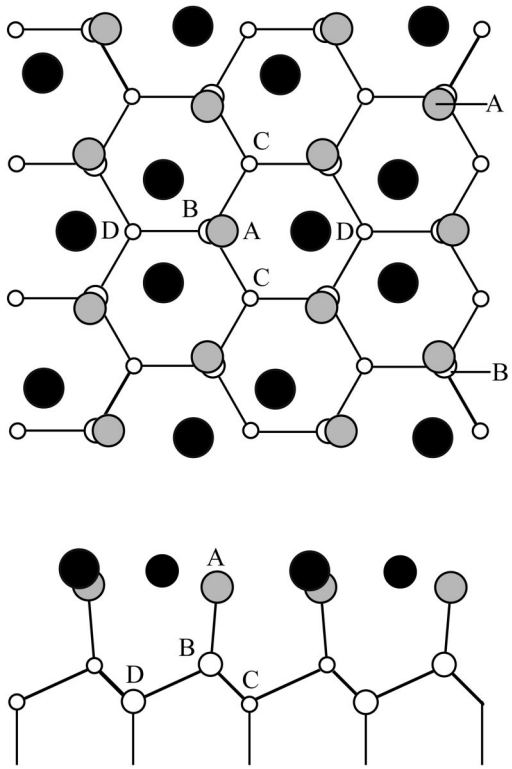

FIG. 3. Top and side view of the CHCT-1 model for the Au/Si(111) $\sqrt{3}\times\sqrt{3}$ surface. The largest circles represent Au atoms while the other circles represent Si atoms. A, B, C, and D indicate different Si sites, which may give rise to surface shifted Si $2p$ components.

is especially evident for the S_2 component, which has an intensity maximum for an emission angle of approximately 20°. Such strong diffraction effects might be expected since the C and B sites, associated with S_1 and S_2 are located much below the Au plane, according to the CHCT-1 model.

From the LEED patterns [Figs. 1(c) and 1(f)] and the Si $2p$ core-level spectra, the β-$\sqrt{3}\times\sqrt{3}$ and the quenched β-$\sqrt{3}\times\sqrt{3}$ phases appear almost identical, despite the difference in coverage. Here we only display the spectra of the quenched β-$\sqrt{3}\times\sqrt{3}$ phase. It is interesting to compare the spectra of the 6×6 surface [Fig. 2(d)] to the quenched β-$\sqrt{3}\times\sqrt{3}$ phase [Fig. 2(c)]. The spectra are all dominated by the bulk component, which determines the Gaussian width to be used in the fitting procedure. A surface component (S_1) is necessary in order to fit the right part of the spectra properly. It is also obvious that S_2 and S_3 has to be introduced to fit the left part of the spectra. The asymmetric shape of the raw spectra at the lower kinetic side motivates the introduction of the surface component S_4.

In similarity with the α-$\sqrt{3}\times\sqrt{3}$ phase, the 6×6 and the quenched β-$\sqrt{3}\times\sqrt{3}$ phases have four surface components (Table I). The core-level shifts of S_1, S_2, S_3, and S_4 are about -0.14, 0.31, 0.57, and 0.90 eV on the quenched β-$\sqrt{3}\times\sqrt{3}$ surface, and -0.15, 0.29, 0.57, and 0.91 eV on the 6×6 surface, with respect to the bulk component. From the raw spectra, it is clear that the quenched β-$\sqrt{3}\times\sqrt{3}$ core-level spectra show more pronounced shoulders than the

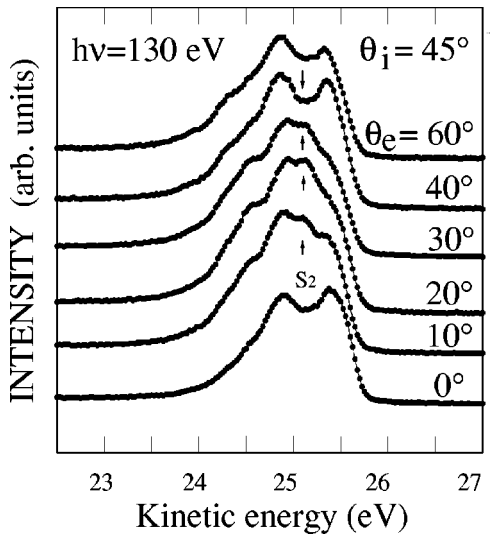

FIG. 4. Si $2p$ core-level spectra recorded from the Au/Si(111) $\alpha-\sqrt{3}\times\sqrt{3}$ surface at different emission angles (100 K). All spectra were obtained with a photon energy of 130 eV at an incident angle of 45°. The arrow points to the intensity change of the S_2 surface component, indicating a strong diffraction effect on this surface.

α-$\sqrt{3}\times\sqrt{3}$ spectra. The Si $2p$ components of the 6×6 phase have smaller Gaussian widths and the surface components are better resolved compared to the quenched β-$\sqrt{3}\times\sqrt{3}$. In agreement with other studies,[11,12] it can be concluded that the quenched β-$\sqrt{3}\times\sqrt{3}$ phase corresponds to a disordered 6×6 phase, since there are clear similarities in the core-level spectra from the two phases. As shown by the previous STM studies,[10–13] the domain walls separate the $\sqrt{3}\times\sqrt{3}$ surface into small areas and the domain wall density is increasing with the Au coverage. In comparison to α-$\sqrt{3}\times\sqrt{3}$, we find that the surface components S_1 and S_3 decrease on the quenched β-$\sqrt{3}\times\sqrt{3}$ surface (60° emission angle). The change might be due to the domain walls, since the domain wall area increases and the $\sqrt{3}\times\sqrt{3}$ area decreases on the quenched β-$\sqrt{3}\times\sqrt{3}$ surface, which means that the number of unaffected Si trimers (S_3) and third layer Si atoms (S_1) might decrease. It is also found that the energy shifts of S_2, S_3, and S_4 are larger for the quenched β-$\sqrt{3}\times\sqrt{3}$ phase than the α-$\sqrt{3}\times\sqrt{3}$ phase.

From earlier STM studies,[10–13] the α-$\sqrt{3}\times\sqrt{3}$ and β-$\sqrt{3}\times\sqrt{3}$ surfaces are quite similar, except for a high domain wall density on the β-$\sqrt{3}\times\sqrt{3}$ surface. Also the β-$\sqrt{3}\times\sqrt{3}$ and 6×6 surfaces are quite similar, except for a crystalline order of the domain walls on the 6×6 surface. On the 6×6 surface, both RHEED and STM (Ref. 13) show the existence of an underlying $\sqrt{3}\times\sqrt{3}$ reconstruction. Furthermore, at high temperature all surfaces show only the $\sqrt{3}\times\sqrt{3}$ reconstruction. It seems reasonable that these surfaces can be regarded as reconstructions caused by extra Au atoms sitting on the $\sqrt{3}\times\sqrt{3}$ substrate surface. Thus the differences between the α-$\sqrt{3}\times\sqrt{3}$, β-$\sqrt{3}\times\sqrt{3}$, 6×6, and the quenched β-$\sqrt{3}\times\sqrt{3}$ surfaces are the positions and the number of extra Au adatoms on the $\sqrt{3}\times\sqrt{3}$ surface (described

by the CHCT-1 model). From the STM images,[13] it seems that the extra Au atoms on the 6×6 surface are located to the Au trimer sites so that the $\sqrt{3}\times\sqrt{3}$ subunits still remain. If this is true, then the β-$\sqrt{3}\times\sqrt{3}$ surface could correspond to a disordered distribution of extra Au atoms (either Au trimer or Si trimer sites, any third choice could be excluded judged from the STM images in Ref. 13). The domain wall areas could be those parts where the extra Au atoms are randomly distributed on either Au trimer or Si trimer sites. If the extra Au atoms are located to the Si trimer sites, the Si $2p$ core level will shift to the higher binding energy side (lower kinetic energy side). This can explain why the energy shifts of S_2, S_3, and S_4 are larger for the quenched β-$\sqrt{3}\times\sqrt{3}$ phase than the α-$\sqrt{3}\times\sqrt{3}$ phase, and also why there are smaller shifts of S_2, S_3, and S_4 for the 6×6 phase compared to the quenched β-$\sqrt{3}\times\sqrt{3}$ phase.

Recently, an interesting pseudopentagonal glass model for the 6×6 phase was proposed by Grozea *et al.*[14,15] based on surface x-ray diffraction data. In this model, a network of incomplete pentagons and trimers forms from the connection of every Au trimer with additional Au atoms. Both the quenched β-$\sqrt{3}\times\sqrt{3}$ and the 6×6 phases come from the high temperature well-defined $\sqrt{3}\times\sqrt{3}$ phase, and the only difference is the cooling process. This behavior is very similar to the glass-crystalline transition in bulk material, indicating that there is a disordered structure on these surfaces, especially for the quenched β-$\sqrt{3}\times\sqrt{3}$ phase. The glass model is basically consistent with the 6×6 to β-$\sqrt{3}\times\sqrt{3}$ transition if the β-$\sqrt{3}\times\sqrt{3}$ phase is assigned to the glass phase. On the other hand, in a local adatom picture, all these surfaces can be regarded as an underlying $\sqrt{3}\times\sqrt{3}$ substrate with extra Au adatoms. At high temperature, the extra Au atoms are highly mobile and they are not trapped by any specific site. Thus the surface shows a well-ordered $\sqrt{3}\times\sqrt{3}$ phase. When the temperature is slowly reduced, Au trimers seem to provide the lowest energy site for the extra Au atoms, resulting in a well-defined 6×6 phase. But when the surface is quickly cooled, the extra Au atoms do not all find a Au trimer site, instead some of them may be trapped by Si trimers, resulting a disordered quenched β-$\sqrt{3}\times\sqrt{3}$ phase (pseudo-$\sqrt{39}\times\sqrt{39}$ phase).

IV. CONCLUSIONS

In summary, photoemission results together with LEED images have supplied an important experimental description of the 5×2, α-$\sqrt{3}\times\sqrt{3}$, β-$\sqrt{3}\times\sqrt{3}$, 6×6, and the quenched β-$\sqrt{3}\times\sqrt{3}$ surfaces. In comparison with earlier reports, a more detailed analysis of the surface contributions to the Si $2p$ core-level spectra has been presented for these surfaces. Three surface components on the 5×2 surface and four surface components on the α-$\sqrt{3}\times\sqrt{3}$, 6×6, and the quenched β-$\sqrt{3}\times\sqrt{3}$ surfaces have been discussed. The reconstructions of the α-$\sqrt{3}\times\sqrt{3}$ phase, the 6×6 and the quenched β-$\sqrt{3}\times\sqrt{3}$ phases have been explained in terms of extra Au adatoms on the $\sqrt{3}\times\sqrt{3}$ surface described by the ideal 1 ML CHCT-1 model. The similarity between the 6×6 periodicity of the 1.1 ML Au surface and its quenched β-$\sqrt{3}\times\sqrt{3}$ appearance is obvious from the fitting results. This behavior is consistent with an order to disorder transition between the 6×6 surface and the quenched β-$\sqrt{3}\times\sqrt{3}$ surface.

ACKNOWLEDGMENTS

Support from the MAX-lab staff is gratefully acknowledged. This work was supported by the Swedish Natural Science Research Council.

[1] L. D. Marks and R. Plass, Phys. Rev. Lett. **75**, 2172 (1995).
[2] R. Plass and L. D. Marks, Surf. Sci. **380**, 497 (1997).
[3] T. Hasegawa and S. Hosoki, Phys. Rev. B **54**, 10 300 (1996).
[4] T. Hasegawa, S. Hosaka, and S. Hosoki, Surf. Sci. **357**, 858 (1996).
[5] A. A. Baski, J. Nogami, and C. F. Quate, Phys. Rev. B **41**, 10 247 (1990).
[6] Y. G. Ding, C. T. Chan, and K. M. Ho, Surf. Sci. **275**, L691 (1992).
[7] R. Plass and L. D. Marks, Surf. Sci. **342**, 233 (1995).
[8] R. Plass and L. D. Marks, Surf. Sci. **357–358**, 42 (1996).
[9] M. Chester and T. Gustafsson, Surf. Sci. **256**, 135 (1991).
[10] J. Nogami, A. A. Baski, and C. F. Quate, Phys. Rev. Lett. **65**, 1611 (1990); **65**, 2211 (1990).
[11] T. Nagao, S. Hasegawa, K. Tsuchie, S. Ino, C. Voges, G. Klos, H. Pfnür, and M. Henzler, Phys. Rev. B **57**, 10 100 (1998).
[12] T. Nagao, C. Voges, H. Pfnür, M. Henzler, S. Ino, F. Shimokoshi, and S. Hasegawa, Appl. Surf. Sci. **130/132**, 47 (1998).
[13] E. A. Khramtsova, H. Sakai, K. Hayashi, and A. Ichimiya, Surf. Sci. **433–435**, 405 (1999).
[14] L. D. Marks, D. Grozea, R. Feidenhans'l, M. Nielsen, and R. L. Johnson, Surf. Rev. Lett. **5**, 459 (1998).
[15] D. Grozea, L. D. Marks, R. Feidenhans'l, M. Nielsen, and R. L. Johnson, Surf. Sci. **418**, 32 (1998).
[16] T. Okuda, H. Daimon, S. Suga, Y. Tezuka, and S. Ino, J. Electron Spectrosc. Relat. Phenom. **80**, 229 (1996).
[17] T. Okuda, H. Daimon, S. Suga, Y. Tezuka, and S. Ino, Appl. Surf. Sci. **121/122**, 89 (1997).
[18] G. Le Lay, V. Yu. Aristov, L. Seehofer, T. Buslaps, R. L. Johnson, M. Göthelid, M. Hammar, U. O. Karlsson, S. A. Flodström, R. Feidenhans'l, M. Nielsen, E. Findeisen, and R. I. G. Uhrberg, Surf. Sci. **307–309**, 280 (1994).
[19] H. M. Zhang, T. Balasubramanian, and R. I. G. Uhrberg, Phys. Rev. B **63**, 195402 (2001).
[20] F. J. Himpsel, G. Hollinger, and R. A. Pollak, Phys. Rev. B **28**, 7014 (1983).